6

INDUSTRIAL CARBON CHEMICAL VAPOR INFILTRATION (CVI) PROCESSES

I. Golecki

1 Introduction

Carbon–Carbon (C–C) fiber-matrix composite materials – C–Cs (Buckley and Edie, 1993; Savage, 1993; Thomas, 1993) possess several extraordinary sets of properties. Foremost, C–Cs have densities in the range of 1.6–2.2 $g\,cm^{-3}$, much lower than those of most metals and ceramics. Lower densities can be translated into lower component weights, an important consideration, especially for applications in flying platforms. C–Cs also have excellent mechanical and thermal properties. The mechanical strengths of C–Cs *increase* with temperature, in contrast to the strengths of the majority of other fiber–matrix composites and those of metals and ceramics, which *decrease* with increasing temperature. C–Cs evidence high toughness and graceful failure under load, as do some other fiber-matrix composites, in contrast to the more abrupt brittle behavior of most monolithic materials. No melting occurs in C–Cs at increasing temperatures, although carbon evaporates above ≈ 2,500 °C. Appropriately processed, pitch-fiber based C–C's possess higher thermal conductivities than copper and silver and they exhibit, by far, the highest thermal conductivity per unit density among thermal management materials, e.g. 400 $(Wm^{-1}k^{-1})/(g\,cm^{-3})$ (Golecki *et al*., 1998). In addition, the thermal expansion coefficient of C–Cs in the fiber direction at 20 °C to ≈1,000 °C is between −1 and 1 ppm/°C, much lower than that of most other structural materials. Consequently, thermal stresses in C–C articles are, in principle, also lower. All of these properties of C–Cs can be tailored by design, using different fibers, matrices, processing methods and schedules. While C–C articles can be used from cryogenic temperatures to over 3,000 °C, and in severe and chemically aggressive environments, they require protection from oxidation for continuous use above ≈350 °C. The practical effect of oxidation is to diminish the structural and functional integrity of the article. Effective engineering solutions for protecting C–C articles from oxidation have been demonstrated for different types of articles and different temperature-time envelopes (Buckley and Edie, 1993; Savage, 1993; Sheehan *et al*., 1994; Golecki *et al*., 2000). Current and potential future applications of C–Cs include disc brake pads for commercial and military airplanes and racing cars, uncooled engine parts, rocket leading-edge sections, furnace heating elements, heat sinks for high-power electronics, heat exchangers, and bipolar plates for proton-exchange-membrane fuel cells.

Carbon–Carbon articles generally comprise (a) continuous or chopped carbon fibers produced from rayon, polyacrilonitrile (PAN) or pitch precursors and (b) one or more types of

carbon matrices (Savage, 1993). One of the most common fabrication methods of C–C articles is densification of a porous preform having the desired shape, so-called near-net processing. The preform consists only or principally of fibers. The initial geometrical density of such preforms varies in the range 10–80% of the theoretical value at full density. Preforms may be fabricated using e.g. weaving of continuous fibers, lay-up of fibrous mats or fabrics, needle-punching, or mixing of chopped fibers with resins and powders, followed, as needed, by thermal treatment in the 200–1,000 °C range to evaporate organic binders or residues (Savage, 1993). Fabricating, cutting and machining a porous preform is easier and faster than machining a fully-dense C–C bar, which often requires diamond tooling. The densification of the preform can be achieved either from the vapor phase, conventionally by means of isothermal isobaric chemical vapor deposition and infiltration (CVD/CVI), or by liquid-phase resin infiltration and annealing, or by a combination of these two approaches. Both approaches involve heating the preforms to about 1,000 °C, either during CVI or after resin has been placed inside the preforms. Conventionally, in either densification approach, several steps are required to effect sufficient densification of the preforms. Minimum final density values are necessary for achieving the desired mechanical and thermal properties. All densification methods leave typically 1–10% of voids in the composite. The average density of a composite article, ρ_{av}, is equal to:

$$\Sigma\rho_i X_i = \rho_f X_f + \rho_{m1} X_{m1} + \rho_{m2} X_{m2} + \cdots \quad (1)$$

where the X_i denote the respective volume fractions ($\Sigma X_i = 1 - X_v$) and the subscripts f, m*i*, and v denote fiber, matrix no. *i*, and void, respectively. After densification is complete, the C–C article may just need to be lightly machined to final tolerances. Additional processing steps involved in the manufacture of C–C articles often include high-temperature (1,000–3,000 °C) annealing in an inert ambient, called graphitization, in order to achieve desired properties, and oxidation protection treatment.

In this chapter, a brief review is provided of CVI routes to the densification of C–C's, from an industrial perspective, with emphasis placed on published approaches demonstrated to reduce the processing time of functional components or that show potential for the same; a more extensive review of this subject was published recently (Golecki, 1997).

2 Overview of carbon CVI

CVI and CVD (Pierson, 1992; Hitchman and Jensen, 1993) involve flowing one or several streams of precursor vapors containing the desired element or compound, e.g. methane (CH_4), over and around the porous parts, while keeping these parts in a furnace at a sufficiently high temperature to decompose the precursor. Each flow rate is usually controlled by means of an electronic mass flow controller and the total pressure in the furnace can be controlled independently by means of a throttle valve, which varies the flow conductance to the vacuum pumps. The terms CVD and CVI are often used interchangeably, but strictly speaking, they denote different processes. The purpose of CVD is to deposit a functional, thin coating on a dense substrate; e.g. the coating may serve as the active part of an electronic device or as a protective layer. The coating produced by CVD generally adds less than 1% of weight to the substrate and the deposition time is of the order of a few minutes to a few hours. The primary purpose of CVI, on the other hand, is to increase the density of a porous body by 100–900%, in order to obtain a material with desirable properties. In addition to achieving the desired density, a specific carbon matrix microstructure may be required,

which is a function of the CVI process conditions. The infiltration time in conventional CVI methods is therefore much longer than the deposition time in CVD.

The most important quantity describing a CVD process is the *deposition rate* of the coating, r, which may vary from $\approx 10^{-2}$–$10^{3}\ \mu m h^{-1}$. The most important parameter influencing the deposition rate for a given material system is the *substrate temperature*. The deposition rate can be expressed (Grove, 1967) as:

$$r = C_g[k_s h_g/(k_s + h_g)]/N_s, \tag{2}$$

where C_g is the chemical concentration in the gas phase, k_s is the rate constant for heterogeneous decomposition of the chemical into the film on the surface of the substrate, h_g is the gas-phase mass-transfer coefficient of the chemical to the substrate, and N_s is a normalizing constant. This chemical may be, but often is not the input precursor (e.g. CH_4) introduced into the reactor. Often a complex series of chemical reactions lead from the input gas to the solid film. The gas-phase mass-transfer coefficient can be expressed as $h_g = D/d_b$, where D is the gas-phase diffusivity and d_b is the thickness of the boundary layer. When $k_s \ll h_g$, $r \approx k_s C_g/N_s$ and the process is *surface-reaction controlled*. Under these conditions, the reaction rate constant k_s and hence the deposition rate r usually increase exponentially with temperature according to the Arrhenius law:

$$k_s = k_{so}\exp(-E_a/kT), \quad r = (k_{so}C_g/N_s)p^n\exp(-E_a/kT), \tag{3}$$

where E_a is the activation energy for the controlling surface reaction, T is the absolute temperature in K, and Boltzmann's constant $k = 1.3805 \times 10^{-16}\ \mathrm{erg K^{-1}} = 8.614 \times 10^{-5}\ \mathrm{eV K^{-1}}$ (see Fig. 6.1). For carbon, $E_a \approx 2 - 4$ eV/molecule. Pressure signifies the pressure in the reactor chamber.

At higher temperature, when $k_s \gg h_g$, $r \approx h_g C_g/N_s$ and the process is *gas-phase diffusion controlled*. Under these conditions, transport of the precursor through the gas phase to the substrate becomes the limiting factor, while the surface chemical kinetics are relatively more rapid. In this regime, the deposition rate increases with temperature much more slowly, as $r = AT^b$, where $b \approx 0.5 - 1$, due to the temperature dependence of the gas-phase diffusivity. At still higher temperature, the deposition rate decreases with increasing temperature, due to competing reactions, such as homogeneous gas-phase nucleation or powder formation and sometimes etching of the surface of the film. Generally, lower temperatures, lower pressures, increased dilution, and higher flow rates (i.e. milder CVD conditions) minimize undesirable processes at the expense of growth rate. The choice of precursor may also influence the deposition rate and the properties of the deposited coating (Tesner, 1984; Duan and Don, 1995; Hüttinger, 2001).

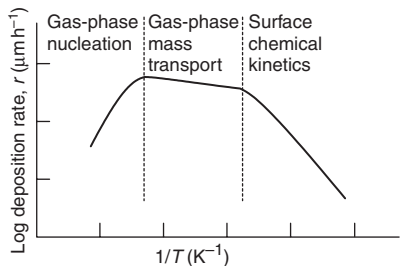

Figure 6.1 Three temperature regimes in chemical vapor deposition.

To sum, the basic steps in CVD are: (1) transport of the gaseous precursor from the center of the gas stream to the boundary layer, (2) diffusion of the precursor across the boundary layer to the surface of the substrate, and (3) decomposition of the precursor on the surface of the substrate to form the solid coating. The last step includes adsorption of precursor-derived moieties on the surface, desorption of other moieties from the surface, surface diffusion and chemical reactions. The conditions during CVD are usually far from thermodynamic equilibrium. Only a few systems, such as Si and GaAs, have been studied in relative depth. An accurate description of the CVD mechanism requires numerically solving the combined chemical and flow equations for the particular reactor configuration. In spite of the progress achieved, quantitative modeling of CVD processes in general cases is limited. Porting of a process from one reactor to another reactor of different geometry and/or size may not be trivial. Therefore, reliable data must be acquired experimentally.

In CVI, an additional gas-phase diffusion step needs to occur after the second step in CVD, namely diffusion from the surface of the preform into the interior pore. Such diffusion may be driven by a concentration gradient (isobaric CVI) or by a pressure gradient (forced-flow CVI). Porous fiber preforms generally have a complex pore size distribution, which may consist of several median size ranges. Continuous fibers, with diameters of 5–15 μm, are arranged in bundles or tows, with 500–3,000 or more fibers per bundle (Lovell, 1995). Pore sizes between individual fibers are of the order of 1–15 μm, those between fiber bundles and between cloth layers are typically 50–500 μm. Because flow conductances are proportional to the opening diameter to the third or fourth power, the partial pressure of a precursor inside a small pore in a preform may be different than its value in the reactor. Also, the characteristic dimensions(s), a, for the reactor (1–500 cm) and for the interior of the preform (1–500 μm) differ by many orders of magnitude. For example, for a mean free path $\lambda = 17\,\mu m$ (methane molecules at 1,000 °C and 10 Torr = 1.3×10^3 Pa), and assuming the same pressure in the pore as in the reactor, the flow would be laminar outside the preform ($\lambda \ll a$) and laminar, mixed or molecular inside a pore in the preform. Therefore, both the gas-phase diffusion and the CVD deposition mechanisms may differ in the reactor and inside a pore: while on the surface of the preform, the CVD process may be in the surface-reaction controlled regime, within an interior pore there may be significant depletion of the precursor due to slow gas-phase diffusion in the molecular regime and the process may be gas-phase diffusion controlled. This state of affairs may lead to non-uniform densification observed in isothermal, isobaric CVI of thick preforms, where the outer surface of the preform has a higher density than the interior regions.

A helpful dimensionless number in CVI is the Thiele modulus (Thiele, 1939):

$$\theta = (k_s L^2/Da)^{0.5} \tag{4}$$

where a and L are the pore diameter and length, respectively. The Thiele modulus gives the relative importance of chemical reaction rate versus gas-phase diffusion. Solution of the pertinent differential equations for mass transfer, diffusion and change of pore geometry under simplifying assumptions results in the following expression for the concentration profile, $C(z)$, of the precursor species along the pore ($0 \leqslant z \leqslant L$):

$$C(z)/C(0) = \cosh[(1 - 2z/L)\theta]/\cosh\theta. \tag{5}$$

As shown in Fig. 6.2, the gas-phase concentration within the pore and therefore the deposition rate of the solid will be more uniform the smaller the Thiele modulus, i.e. the larger the gas-phase diffusivity compared to the surface reaction rate, and the smaller the aspect ratio L/a. It is generally preferable in CVD and CVI to operate in the surface-reaction controlled

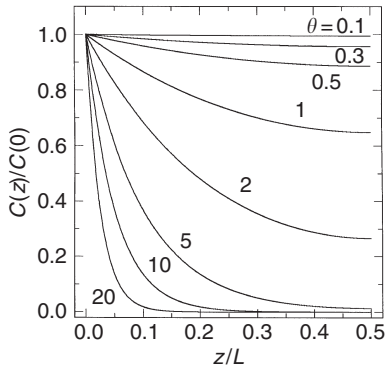

Figure 6.2 Calculated relative deposition rate along a pore axis, z, for different values of the Thiele modulus, θ; L = pore length.

regime, where D/k_s is large. For Fickian diffusion, the diffusivity D is inversely proportional to pressure and thus operating at lower pressures will decrease θ and result in a more uniform infiltration profile (Kotlensky, 1973; Naslain *et al*., 1989; Pierson, 1992; Savage, 1993) and a more uniform microstructure (Pierson and Lieberman, 1975) in the pore. The value of the Thiele modulus will change during infiltration, because both the gas-related quantities and the aspect ratio of the pore will change. The above simplifying assumptions include a first-order chemical reaction with no change in volume and no homogeneous gas-phase reactions; solutions for other cases were published (Thiele, 1939). In many CVI processes, including carbon CVI, there is a net increase in the volume of the gaseous materials due to the decomposition of the precursor. Thus, fresh precursor species have to diffuse into the pores against an opposite, higher flow of by-product species. For carbon CVI, temperatures can vary, e.g, in the 600–2,000 °C range, depending on the particular chemistry and system; total pressures in the reactor are generally in the range $0.13 - 1.3 \times 10^5$ Pa ($10^{-3} - 10^3$ Torr).

CVI has several advantages compared to other densification methods. CVI allows penetration of the desired atoms or molecules into the smallest pores of the preform and does not require post-densification treatment to remove organics. CVI produces uniform and conformal coatings around each accessible fiber and surface in the preform. The matrix produced by CVI is purer than that obtained by hot pressing. The final shape of an article densified by CVI is closest to the desired shape. CVI minimizes the mechanical damage to the fibers as a result of the much lower pressures and temperatures employed. The published methods described here of infiltrating composites using CVI are listed in Table 6.1 and depicted schematically in Fig. 6.3 (Golecki, 1997). These CVI methods can be divided into several categories, depending on:

(i) spatially uniform temperature (isothermal) or not (thermal gradient);
(ii) heating method – radiative or inductive;
(iii) type of reactor – cold wall or hot wall;
(iv) method of extraction of heat from the preform (e.g. radiative, convective, conductive);
(v) pressure regime – atmospheric or low pressure;
(vi) uniform pressure (isobaric) or pressure gradient (forced flow, pulsed pressure);
(vii) whether a plasma is used;
(viii) whether immersion in a liquid is required.

Table 6.1 Published characteristics of different chemical vapor infiltration methods used to densify C–C composite articles and described in this chapter

CVI process (Section no.)	*Preform*		*Process*			*Reactor*	
	Multiple	*Thick/large size (>2.5 cm in all directions)*	*Densification time (w/r to perform thickness)*	*Pressure adjustable*	*Precursor efficiency*	*Cost of capital*	*Special fixturing*
Isothermal isobaric (2.2)	Yes	Yes	Very long	Yes	Low	High	No
Early thermal-gradient inductively-heated isobaric (2.3.1)	No	Yes	Long	Yes			Yes
Recent thermal-gradient inductively-heated isobaric (2.3.2)	Yes	Yes	Short	Yes	High	Low	No
Liquid-immersion thermal-gradient inductively-heated isobaric atm. pressure (2.4)	No	No	Short	No			
Forced-flow thermal-gradient (2.5)	No	No	Short	Very limited	High	Low	Yes

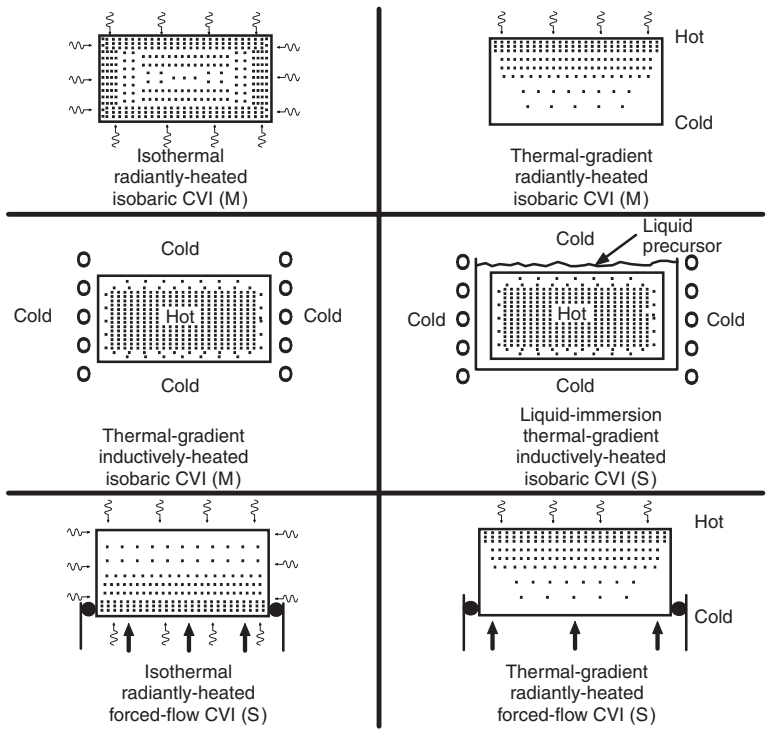

Figure 6.3 Principles of the main chemical vapor infiltration methods (Golecki, 1997); M = multiple preforms, S = single preform per run.

Different CVI methods are at different stages of technological and industrial maturity. Much data on infiltration of composites are unpublished or unavailable. Thus, the comparisons provided in this chapter are based on printed, public-domain studies, and patents. In the next sections, more detailed consideration is given to specific CVI methods used in fabrication of C–C articles.

3 Chemical vapor infiltration processes

3.1 Isothermal isobaric carbon CVI

Isothermal isobaric CVI is in wide use since the 1960s for densification of C–Cs and other refractory composites (Kotlensky, 1971; Savage, 1993; Golecki, 1997). In a common application, a large number of porous carbon disk brake-pad preforms, typically 15–55 cm in outer diameter (o.d.) by 2–3 cm in thickness, are placed in a hot-wall reactor, i.e. a furnace uniformly heated by radiation, at a temperature in the range 1,000–1,100 °C and exposed to a flow of reactant gas, e.g. CH_4 at 5–100 Torr = $6.6 \times 10^2 - 1.3 \times 10^4$ Pa (Thomas, 1993); see Fig. 6.4. In isothermal isobaric CVI, the densification kinetics of a thin (e.g. 1–2 mm thick) preform with initial density ρ_o follow an exponential approach with time to a "final" density value, ρ_f (Loll *et al*., 1977; Marinkovic and Dimitrijevic, 1987; Naslain *et al*., 1989):

$$\rho(t) = \rho_o + (\rho_f - \rho_o)[1 - \exp(-t/\tau)] \tag{6}$$

where τ is the time constant of the process; τ decreases with increasing temperature according to an exponential (Arrhenius) relationship in the surface-reaction limited regime. For such a thin preform, ρ_f may equal the desired final density, but in a thicker preform the surface pores become clogged well before that density value is reached, requiring several interruptions of the infiltration to allow grinding the external surfaces in order to open the pores and enable further infiltration; see Fig. 6.5. The total densification time is thus a strong supra-linear function of the thickness of the preform. For > 2 cm thick preforms, 600–2,000 h may be required to achieve the desired density.

Since from an economic viewpoint, it is desirable to minimize the densification time, higher temperature and precursor pressure would seem to be the direction to follow. However,

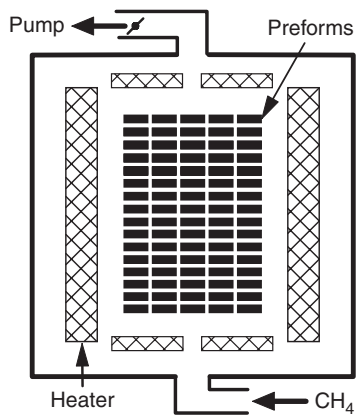

Figure 6.4 Simplified schematic diagram of a hot-wall, isothermal–isobaric chemical vapor infiltration reactor (not to scale).

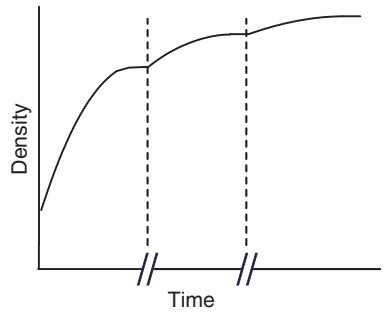

Figure 6.5 Schematic illustration of the densification kinetics of a thick preform in isothermal isobaric chemical vapor infiltration.

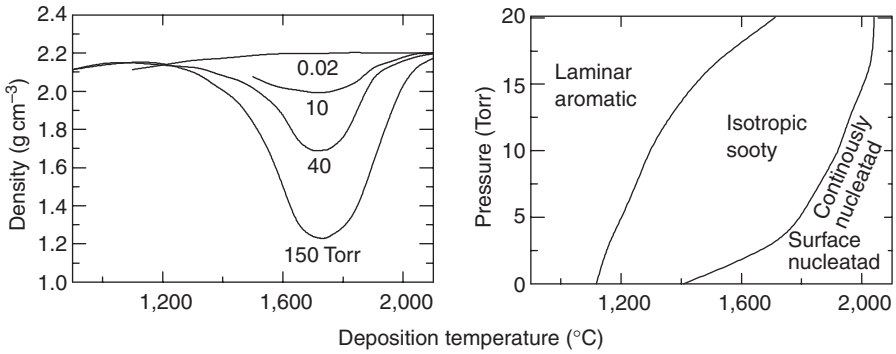

Figure 6.6 Density and microstructure of infiltrated carbon versus temperature and pressure (Kotlensky, 1971; reprinted by permission of the Society for the Advancement of Materials and Process Engineering).

doing so may also lead to more premature closure of surface pores. Conversely, lower temperatures and pressures may reduce undesirable gas-phase nucleation and formation of tar and soot by-products. Lower pressure corresponds to higher gas-phase diffusivity, leading to more uniform distributions of density and microstructure within the composite. For example, the density minimum observed in carbon CVI (Kotlensky, 1971) – see Fig. 6.6 – was interpreted as resulting from the incorporation of soot particles formed in the gas phase into the carbon deposited in the pores of the preform. If the pressure was reduced sufficiently, this density minimum could be eliminated. C–C composites having larger crystallite size, L_a, and improved thermal and electrical conductivities were produced at lower pressures (Stoller and Frye, 1972). Rough-laminar (anisotropic) carbon, which is generally desired for many applications, was obtained at 35 Torr (4.7×10^3 Pa), but not at 100–760 Torr ($1.3 \times 10^4 - 1.0 \times 10^5$ Pa). Rough-laminar carbon can be rendered more graphitic, i.e. more ordered microstructurally, by high-temperature treatment (graphitization) at $\geq 2{,}000\,^{\circ}\mathrm{C}$ (Loll *et al*., 1977) and this may result in improved composite properties. Lower pressures also allow lower inlet precursor flow rates.

The effect of different precursors on the carbon densification rate of $7.6 \times 7.6 \times 1.6$ cm carbon preforms was studied (Duan and Don, 1995). Randomly oriented pitch-fiber tow preforms were impregnated with phenolic resin and densified at 1,000–1,150 °C and 15 Torr

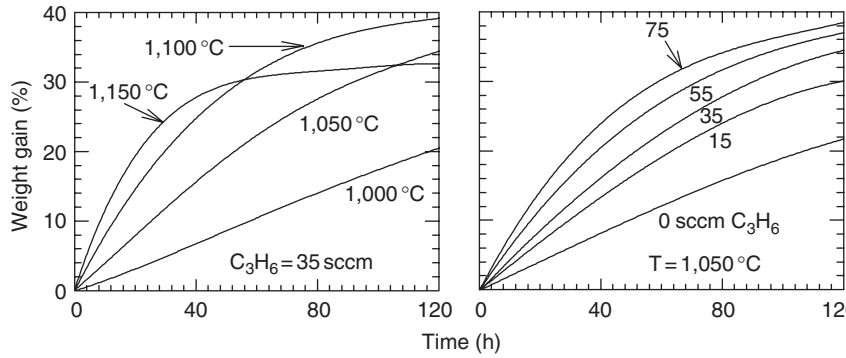

Figure 6.7 Relative weight gain versus time in isothermal isobaric carbon CVI from CH_4 and H_2, showing the effects of temperature and C_3H_6 additions (Duan and Don, 1995; reprinted with the authors' kind permission).

(2.0×10^3 Pa). The initial density and open porosity of the preforms were 1.25 g cm^{-3} and 38 vol%, respectively. The preform weight was continuously recorded by means of an in-situ balance. CH_4 at 400 sccm was the primary precursor, with additions of 100 sccm H_2 and 0–75 sccm propylene, C_3H_6. The hot zone of the furnace was 15.2 cm in diameter by 30.5 cm long. The curves of fractional weight gain versus time had an exponential-type behavior and were fitted to the equation $\Delta m/m = a_1(\rho_{CVD}/\rho_o)\ln\{1 + a_2[\exp(-a_3 t - a_4 t^2)] - 1\}$, where the a_j's were constants. At 1,050 °C, the addition of increasing fractions of C_3H_6 resulted in increases of the initial deposition rate and of the final density, shown in Fig. 6.7. The microstructure of the deposited carbon changed from isotropic in the absence of C_3H_6 to anisotropic when 35 sccm C_3H_6 was added. With 35 sccm C_3H_6, increasing the temperature from 1,000 to 1,100 °C also increased the initial densification rate and the final density, whereas at 1,150 °C, premature surface pore closure and non-uniform deposition through the thickness were seen.

Thus, the operating conditions of a hot-wall, isothermal isobaric CVI process involve a compromise which results in materials with the desired properties in the shortest possible time and with the minimum amount of labor, supplies, and energy.

Advantages of isothermal isobaric CVI include:

- The method is well-established and relatively well-understood.
- A large number of preforms can be densified simultaneously.
- The densification time per preform is relatively low for heavy loading of the reactor.
- Preforms of different and complex shapes and sizes can be readily densified in the same run, although the minimum dimension (usually the thickness) needs to be similar.
- The energy expenditure per part is relatively low.

Disadvantages of isothermal isobaric CVI include:

- Premature surface crusting occurs before the desired bulk density is reached, necessitating several interruptions in the CVI process to grind surfaces.
- Very long hot processing time, typically 600–2,000 h per batch (but the time does not depend on the number of parts being densified in a given reactor).
- The density within the article is generally highest at the surfaces and lowest in the interior regions.

- Overall precursor conversion efficiency is low, of the order of 1–2%.
- Preforms having different minimum dimensions (usually the thickness) densify at very different rates.
- Capital cost is relatively high.
- Cost of inventory and potential re-work can be high.
- Process development or process changes may be slow to implement.

From the previous sections, it follows that in order to significantly speed up the densification process of relatively thick parts, either the temperature or the pressure during CVI has to be increased, yet without clogging surface pores or degrading material properties. The next section describes approaches using a thermal gradient to achieve this goal.

3.2 Thermal-gradient inductively-heated isobaric CVI

3.2.1 Early thermal-gradient isobaric CVI studies

In an early thermal-gradient CVI process (Stoller and Frye, 1972; Lieberman and Noles, 1973; Stoller *et al*., 1974; Lieberman *et al*., 1975), intended for rocket components (Thomas, 1993), a porous carbon felt was mounted around a truncated-conical graphite susceptor; see Fig. 6.8. This electrically conductive susceptor was heated by a conical-shaped induction coil (frequency and power levels not provided). The felt was fabricated using 5 cm long, chopped oxidized PAN fibers, which were carded into batts (Lieberman *et al*., 1975). Alternate carded batts were cross-plied when they were felted by means of a needle loom, in an effort to achieve isotropic properties in the plane. The felts were nominally $118 \times 118 \times 3.2$ cm in size and had a density of $0.14 \pm 0.02\,\mathrm{g\,cm^{-3}}$. Each felt, which was initially flat, was made into a truncated hollow cone by sewing a single seam along the entire length of the cone with a rayon-based carbon yarn. After carbonization in flowing Ar to 1,300 °C to remove volatiles, the weight loss was 44% and the linear shrinkage 13.5–14.6%. The carbon deposition conditions of one preform were (Lieberman *et al*., 1975): susceptor temperature = 1,325 °C, total pressure = 8.4×10^4 Pa (= 630 Torr = 1 atm in Albuquerque, NM), CH_4 flow rate = 61 $\mathrm{l\,min^{-1}}$, Ar flow rate = 205 $\mathrm{l\,min^{-1}}$ and free gas space between shroud and preform = 2.5 cm. From the description given (Lieberman and Noles, 1973; Stoller *et al*., 1974; Lieberman *et al*., 1975) it appears that the felt did not initially couple electrically to the coil, so there was no induced electrical current flowing around the circumference of the felt. The sewn construction of the felt may have resulted in a very high electrical resistivity in the circumferential direction and thus a lack of initial electromagnetic coupling. The heating of the felt therefore occurred initially by thermal radiation. It was stated (Stoller *et al*., 1974) that carbon was deposited first at the surface of the felt adjacent to the susceptor and then deposition progressed radially through the preform as the densified preform became inductively heated. However, as reported (Stoller and Frye, 1972; Stoller *et al*., 1974), a reduction by a factor of two only was achieved in the overall densification cycle time, compared to isothermal CVI, and this technique was limited to densifying one preform at a time. Gas analysis data (Lieberman and Noles, 1973) indicated that densification times were equal to or longer than 130 h; infiltration times of six weeks (1,000 h) were reported (Lackey, 1989). This process also suffered from soot formation due to the combination of the very high temperature and high pressure employed. Spatial density distributions were obtained from samples cored through the thickness of the frustum. There was a density gradient from the inner

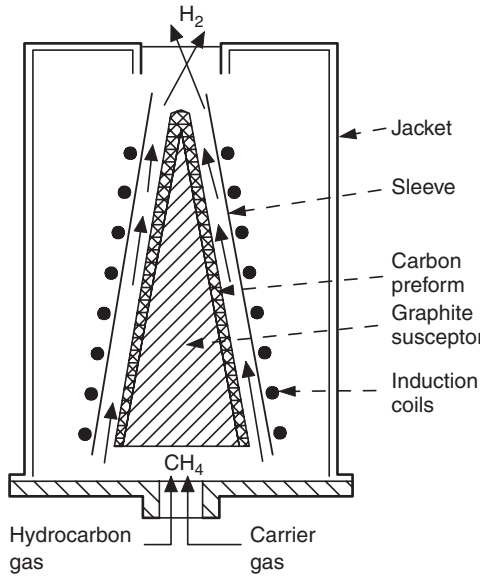

Figure 6.8 Schematic diagram of an early thermal-gradient CVI system (Stoller and Frye, 1972; *reprinted by permission of the Society for the Advancement of Materials and Process Engineering*). The axially sewn preform did not couple to the coil or its coupling was very inefficient and it was thus initially heated by thermal radiation from the inductively-heated conical susceptor.

half (1.73–1.84 g cm^{-3}) towards the outer half (1.87–1.89 g cm^{-3}) of the wall thickness (Lieberman *et al*., 1975), as in isothermal isobaric CVI, indicating possible surface crusting. Significant density gradients were measured for infiltrations performed at lower temperatures (Stoller *et al*., 1974). The microstructure, as measured in polarized-light microscopy, was rough-laminar in 70–100% of the outer half of the wall thickness; the remainder was smooth-laminar, which also comprised an outer, 0.2 cm crust (Lieberman *et al*., 1975). In the inner half, 40–60% of the matrix was rough-laminar.

Advantage of early inductively heated thermal-gradient isobaric CVI process is:

- A decrease of the infiltration time by a factor of about two, compared to isothermal isobaric CVI.

Disadvantages of early inductively-heated thermal-gradient isobaric CVI process include:

- A relatively long infiltration time.
- Spatial gradients in density and microstructure within the thickness of the preform.
- No easy control of deposition and infiltration conditions.
- Large, expensive, specifically machined graphite susceptor was required because of lack of inductive coupling between the induction coil and the preform at the start of infiltration.
- Only one preform densified per run.
- Possible need to machine the cooler, insufficiently-infiltrated surface after the run.
- Preforms having significantly different shapes or dimensions may require different coil and susceptor configurations.

In the next section, recent developments are described which demonstrated at least a ten-fold reduction in the densification time of multiple, thick C–C composites through efficient electromagnetic coupling to an induction coil.

3.2.2 Recent inductively-heated thermal-gradient isobaric CVI studies

Recently it was demonstrated that three 10.8 cm o.d. × 4.4 cm i.d. (internal diameter) × 3.0 cm thick PAN-carbon-fiber preform disks, having an initial density of 0.4–0.6 g cm^{-3}, could be directly heated by electromagnetic induction and simultaneously densified in 1 to 2 days (Golecki *et al*., 1994; Golecki *et al*., 1995a). A novel, in situ, densification-rate monitor was also developed (Golecki and Narasimhan, 1998). The thermal-gradient C–C CVI system is shown schematically in Fig. 6.9. The main part of the water-cooled, stainless steel deposition chamber was 38 cm i.d. × 43 cm high. A 38 cm high conical flange allowed access from the top of the chamber. The chamber was pumped by means of a Roots blower, backed by a chemically resistant rotary forepump. The exhaust from the forepump was connected to an oxidation furnace. Flowing cyclopentane, C_5H_{10}, was delivered to the bottom of the chamber as a vapor through a mass-flow-controlled gas line maintained at 70 °C. C_5H_{10} is a liquid at 25 °C with a vapor pressure of 4.3×10^4 Pa (321 Torr) and a boiling point of 50 °C; in large quantities it costs about \$0.44 kg^{-1}. Being a liquid, it occupies significantly less storage space than a gaseous carbon precursor. The total pressure in the deposition chamber was measured using a diaphragm pressure gauge and controlled by means of electronically operated throttle valves. The process ranges were: total pressure = 20 − 100 Torr ($2.7 \times 10^3 - 1.3 \times 10^4$ Pa) and C_5H_{10} flow rate = 170 − 540 sccm.

The three thick carbon preforms were placed around a 4.4 cm o.d. molybdenum or alumina (Al_2O_3) centering mandrel and vertically spaced about 1 cm apart. The preforms and

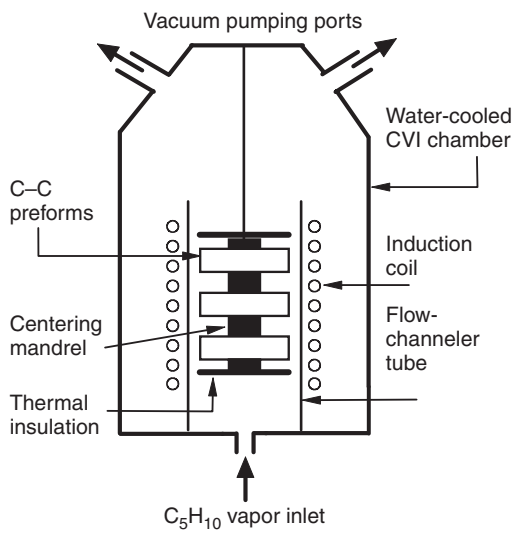

Figure 6.9 Simplified schematic (not to scale) of recent, patented, inductively heated thermal-gradient CVI reactor (Golecki *et al*., 1994; Golecki *et al*., 1995a,b), depicting, as an example, three C–C disk-shaped preforms mounted around a centering mandrel inside an induction coil.

mandrel assembly was centered inside a 15 cm i.d. × 22 cm long, helical, water-cooled copper induction coil placed inside the deposition chamber. An electrically conductive mandrel was not required, as the electrical conductivity of these preforms in the undensified state was sufficiently high to couple directly to the electromagnetic field induced by the energized coil. This was evidenced both by inductively heating such preforms in the coil without any mandrel, by using the electrically insulating alumina mandrel during rapid densification runs, and by densifying other, 5.6 cm thick carbon preforms with no mandrel (Golecki and Narasimhan, 2001).

In order to reduce radiative heat losses from the outer surfaces of the top and bottom preforms, several 11 cm o.d. × 0.06 cm thick grafoil plates were placed above and below the bottom surfaces of the mandrel. In some runs, a 47 cm high × 14.1 cm o.d. × 13.5 cm i.d. quartz tube was inserted between the C–C preforms and the coil, in order to act as a flow channeler for the C_5H_{10} vapor. In other runs, an 11.4 cm high quartz tube was placed between the bottom of the chamber and the coil, so that in this case the surfaces of the C–C preforms were in direct optical communication with the coil and chamber walls. The turnaround time for substrate loading and unloading was very short. The temperatures of the C–C disks were measured directly with 0.25 mm diameter, Pt-13%Rh/Pt thermocouples inserted at different radial locations half-way through the thickness of the disks. Pyrometry measurements were also performed.

The induction coil was energized with an audio-frequency power supply; the power, voltage and frequency could be read from panel meters and recorded electrically during CVI runs. The current in the induction coil was monitored during CVI runs via a device termed the "vacuum thermocouple" (VTC), which was part of the power supply. The VTC readout was derived from a pick-up coil placed around a lead within the power supply, which was connected to the induction coil in the chamber. Therefore, the readout of the VTC was directly related to the current in the coil. The parameter ranges of the power supply were: power = 8.8 − 13.2 kW, frequency = 4.9 − 8.6 kHz.

Figure 6.10 illustrates overall gross densification rates measured by interrupting CVI runs (Golecki *et al*., 1994, 1995a). Average carbon pick-up rates per disk of 9.5 g h^{-1} or 10.6% h^{-1} were obtained. The whole-disk density was increased from 0.41 to 1.54 g cm^{-3} in just 26 h, representing an average rate of increase of 0.044 g cm^{-3} h^{-1}. Overall disk densities of 1.68 g cm^{-3} were obtained, with 1.84 g cm^{-3} in regions, depending on process conditions (PAN carbon fiber density is 1.73 g cm^{-3}). Importantly, the shape of the density vs. time curves was sigmoidal-linear rather than the much slower exponential approach to final density observed in isothermal isobaric CVI. Generally, the highest density was found in the middle disk in the stack, due primarily to lower temperatures at the outer surfaces of the two extremal disks. Optimized end-insulation and coil design can reduce such axial disk-to-disk variations, especially in a scaled-up stack containing, e.g. 30–60 disks. The density uniformity within a disk, as measured from cored and sliced samples, was within ± (5–8)%. The overall conversion efficiency of the precursor, i.e. the amount of carbon added to the disks divided by the amount of carbon which flowed as C_5H_{10}, was 20–30%, over ten times higher than reported for isothermal isobaric CVI, and also higher than published for forced-flow thermal-gradient CVI of carbon (Lackey *et al*., 1995; Vaidyaraman *et al*., 1995b), described in Section 2.5.

Figure 6.11 illustrates the variation of temperature at three radial locations in the middle C–C preform disk during a CVI run. Initially the i.d. region of the disk was hottest, all three temperatures increased as a function of time, and the temperature difference between the i.d. and o.d. decreased as a function of time. Temperatures inside the disk reached almost

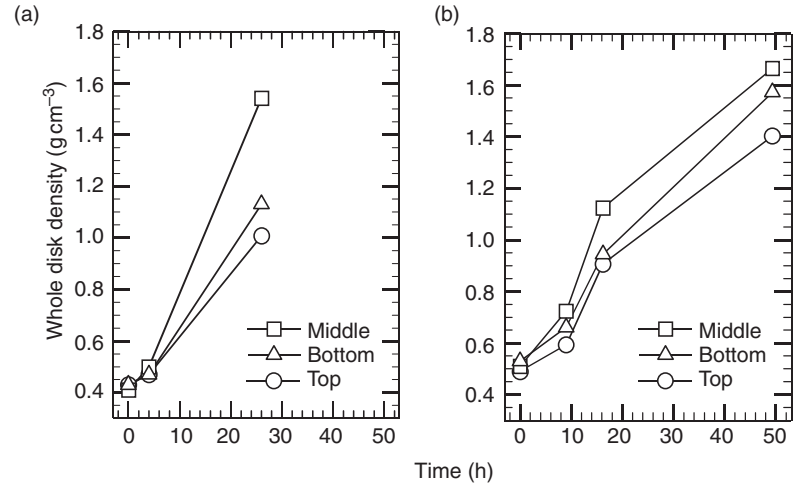

Figure 6.10 C–C disk density versus time in inductively-heated thermal-gradient CVI (Golecki *et al*., 1994): (a) One set of disks, without grafoil insulation, with long flow channeler tube; run was interrupted to weigh the preforms; (b) Three sets of disks in three separate runs, with grafoil insulation, without flow channeler tube. Lines are intended as an aid to the eye.

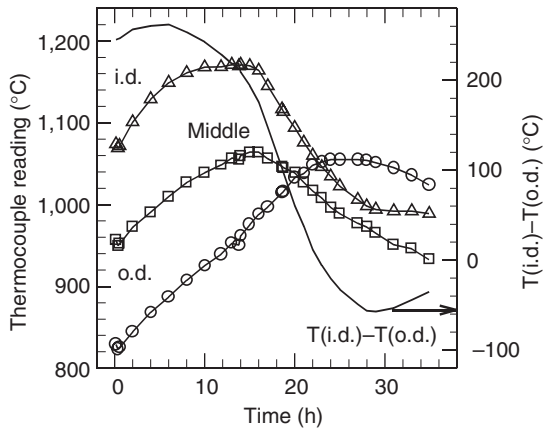

Figure 6.11 Temporal variation of the temperatures at three radial locations in the middle carbon preform disk in a three-disk stack during inductively-heated thermal-gradient CVI (Golecki *et al*., 1995a). Thermocouple inserted: Δ = near inner diameter (i.d.) of preform disk, □ = mid-way between inner and outer diameters, ○ = near outer diameter (o.d.). Solid line without symbols represents the difference between the readings of the inner diameter and the outer diameter thermocouples.

1,200 °C, ≈ 200 °C higher than in isothermal isobaric CVI of carbon. Some surface crusting occurred and yellow vapors were observed in the chamber towards the end of this particular run but these effects were absent in CVI runs stopped earlier. The total amount of liquid tar was significantly smaller in such runs, compared to the estimated 1–3% of the incoming C_5H_{10} for runs which were continued past surface crusting. No solid or powdery soot was found in any of the runs.

Spatial density distributions in C–C disks as a function of infiltration time were obtained from the geometrical dimensions and weights of cored and sliced samples. The measured densities in a middle disk from a three-disk run interrupted intentionally after 9.0 h (approximately quarter-way through the run) are plotted in Fig. 6.12. The densities were highest in the *interior* regions of the disk, both radially and axially. Figure 6.13 shows spatial density distributions measured in a different disk from another run which was intentionally interrupted after 16.2 h (approximately mid-way through that run). Again, the densities were highest in the *interior* regions of the disk and lower near all outside surfaces, whether on the circumferences or on the top and bottom surfaces. Furthermore, the difference between the highest and lowest densities here was only 10%. As the CVI run progressed, regions which had densified less tended to catch up with regions which had densified more.

The microstructure of the deposited carbon was determined by measuring the extinction angle of the Maltese cross in a polarized-light microscope (Savage, 1993). Depending on processing conditions, rough-laminar (19–23°), smooth-to-rough-laminar (13–15°) or smooth-laminar (10–12°) microstructure was obtained. The rough-laminar structure has the highest density and is generally desired for braking applications. Isotropic carbon (0°) was not found. The compressive strength, measured for 6.6 mm diameter × 7.9 mm long samples, increased steeply with increasing density (Golecki *et al*., 1995b). At 1.79 g cm^{-3} the value of the compressive strength was 268 MPa (39 ksi), considered very good.

In this inductively-heated thermal-gradient isobaric CVI process, the substrates were Joule heated by circumferential induced currents flowing inside them. In this geometry, the induced power was initially highest near the o.d. and diminished to zero in $\approx 3\delta$, where the skin depth $\delta = 5(\rho_{el}/f)^{0.5}$ (Brown *et al*., 1948), with δ in cm, the electrical resistivity ρ_{el} in mΩ cm and the frequency f in kHz. For example, for a material with an initial uniform electrical resistivity $\rho_{el} = 10\,\text{m}\Omega\,\text{cm}$, $\delta = 5$ cm at 10 kHz. The substrate temperatures increased with power to the coil. The temperature distribution in the substrates was dominated by the radiation losses, Q, to the water-cooled coil and walls, $Q = \varepsilon\sigma_o(T^4_{os} - T^4_{wall})$, where ε is the emissivity, $\sigma_o = 5.67 \times 10^{-8}\,\text{J K}^{-4}\text{m}^{-2}\text{s}^{-1}$, T is in K and the subscript 'os' denotes outside surface. The temperature would thus initially be highest in the interior regions of the preforms, lower at the top and bottom surfaces and lowest at the o.d., the latter surfaces having the largest view factors of the water-cooled coil and chamber walls.

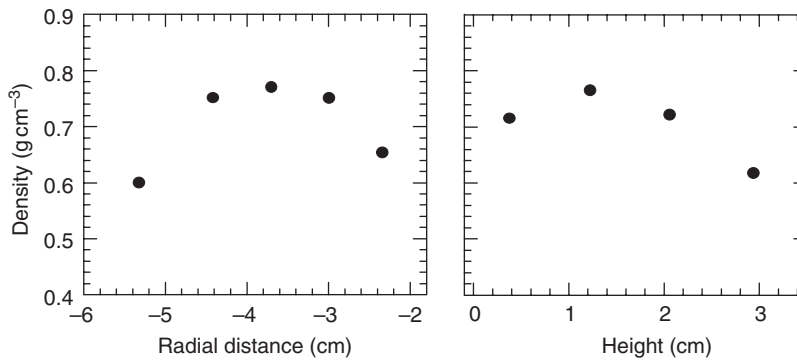

Figure 6.12 Radial and axial density distributions in the middle C–C preform disk in a three-disk stack infiltrated for 9.0 h by inductively-heated thermal-gradient isobaric CVI (Golecki *et al*., 1996).

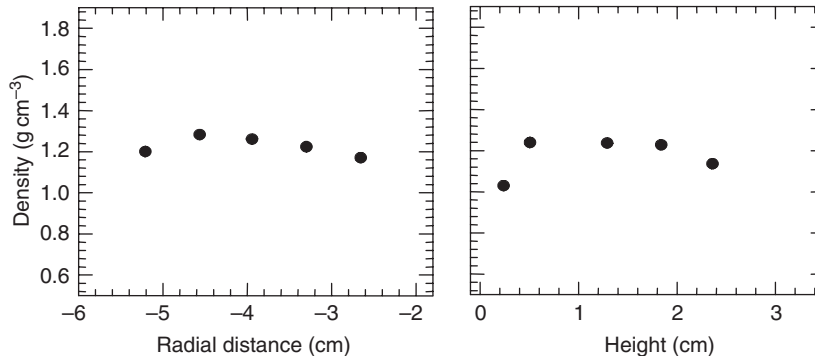

Figure 6.13 Radial and axial density distributions in the middle C–C disk in a three-disk stack infiltrated for 16.2 h by inductively-heated thermal-gradient isobaric CVI (Golecki *et al*., 1996).

The gas-phase diffusivity of the precursor was high, due to the low deposition pressure, ensuring that the initial densification rate would be highest in those hottest interior regions, consistent with the measured spatial density distributions. As densification progressed, the electrical and thermal conductivities of the preform increased. A higher electrical conductivity resulted in a shallower skin depth and improved coupling to the coil, i.e. higher induced current and higher temperatures near the exterior surfaces of the preform, as measured, other conditions being equal. Thus a spatial "inside-out" densification front existed in the preforms. As the pores inside the disk became smaller and finally the surface started crusting, the carbon deposition rate decreased, due to the much smaller available surface area, and the temperature distribution became more uniform.

In situ densification-rate measurements. The rate at which carbon mass was added to the carbon fiber preforms and the total carbon mass added were determined in real time by measuring the current in, or the voltage across, the induction coil; see Fig. 6.14 (Golecki and Narasimhan, 1998). When the induction power supply is run in the constant-power mode, the coil current and voltage will be adjusted to compensate for changes in the coupling to the load, which comprises the carbon-fiber preforms. When the coupling improves, less current (and voltage) is required in the coil to transfer the same amount of power to the preform disks. Referring to Fig. 6.14, both the VTC voltage (which increases with coil current) and the coil voltage decrease with time during inductively-heated thermal-gradient CVI. The initial slopes are approximately constant in this example. At about 14 h into the process, there is a noticeable break in both slopes and from that point on, both slopes are slightly less than one-third of their previous values. The time at which the break in either slope occurs coincides with the time when the i.d. and middle temperatures of the middle disk peak (Fig. 6.11). In CVI runs which were stopped close to the time of the break in slopes, no surface crusting of the preforms was observed. In runs which were continued well beyond the time of the break in the slopes, some surface crusting of the preforms was noted. Furthermore, the amount of liquid tar (a by-product of any carbon CVI process) was significantly reduced in runs terminated at the slope breakpoint. Note, however, that the amount of tar in inductively heated thermal-gradient CVI is generally significantly lower than that in equivalent runs done by conventional, isothermal isobaric CVI. Another point is that even

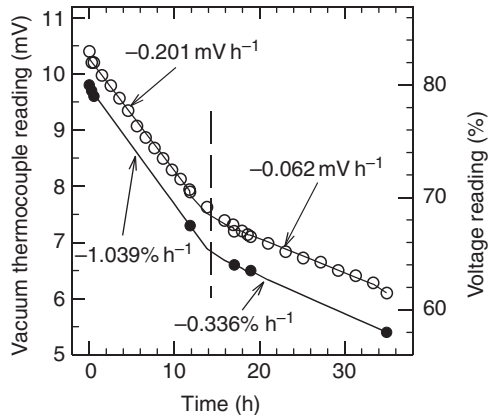

Figure 6.14 Variation of the vacuum thermocouple voltage (○) and coil voltage (●) during inductively-heated thermal-gradient isobaric CVI of three carbon-fiber preforms, each 10.8 cm o.d. × 4.4 cm i.d. × 3.0 cm thick (Golecki and Narasimhan, 1998). Data are for the same run as in Fig. 6.11.

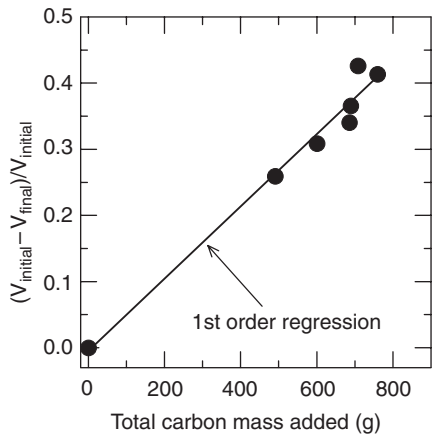

Figure 6.15 Dependence of relative change in vacuum thermocouple readings on the total measured carbon mass added to the three nonwoven PAN-based carbon-fiber preform disks by inductively-heated thermal-gradient isobaric chemical vapor infiltration (Golecki and Narasimhan, 1998). Each point denotes a separate densification run with a different set of preforms.

though the spatial temperature distribution within the preforms changes with time during densification, the intrinsic electrical conductivity of pure carbon or graphite as a function of temperature is constant to better than 4% from 800 to 1,200 °C. Thus, the measured changes in coil current and voltage are due to the increase in carbon mass. Therefore, the slope of either the VTC voltage or the coil voltage as a function of time is a measure of the densification rate. This method is intrinsically very sensitive; e.g. for the case of three carbon preform disks described here, the sensitivity factor is about 0.1 g carbon, or 0.01% of the total mass of carbon added, per μV output of the VTC. When the densification of the bulk of the preforms is complete and surface crusting starts, there is a significant decrease in the slope of both coil current and coil voltage, which can be used as an input signal to terminate the CVI run.

Figure 6.15 illustrates another useful aspect of this novel monitoring and control method. Referring to the rapid densification of the three carbon-fiber preform disks, there is a visual linear relationship between the relative change in VTC readings and the total carbon mass added by CVI to the three disks. This relationship can be used as a calibration curve that makes it possible to apply predictive control of both the densification rate and the process end-point in real time. For example, a preset value of added mass may be identified at the beginning of the densification process. By monitoring the VTC voltage or the coil voltage throughout the process, and using one or the other voltage as an input signal to a feedback control loop, one can control the rate at which the densification proceeds and also end the densification run at exactly the desired time.

Both this thermal-gradient inductively-heated densification process and the densification rate monitoring method described here can be used with different materials systems, article shapes, CVI methods and other processes, for a variety of applications.

Advantages of this recent inductively-heated thermal-gradient isobaric CVI include (Golecki *et al*., 1994; Golecki and Narasimhan, 1998):

- Single-cycle densification – no need for intermediate sanding.
- At least 10 times faster than isothermal isobaric CVI.
- Multiple preforms can be readily densified in one run.
- Thick preforms (>3 cm in thickness) can be densified readily with very good density uniformity.
- Multiple preforms having different thicknesses can be densified in the same run.
- The process is run at low pressure, which results in higher gas-phase diffusivity and is more conducive than atmospheric pressure CVI to obtaining uniform density profiles and formation of matrices and composites with desirable properties.
- All CVI process conditions, including pressure, flow rate, precursor type, precursor dilution, and temperature are fully adjustable in real time.
- High precursor conversion efficiency (20–30%) is obtained without forced flow.
- No solid by-products (only a small amount of liquid tar) are formed.
- Continuous real-time monitoring and control of densification rate and process end-point.
- No fundamental technical barriers exist in scaling up both the preform size and the number of preforms per run.
- Well suited for small or medium batch size for "just-in-time" production with turn-around time of less than one week, reducing inventory and potential scrap rate.
- No special fixturing is required.
- No extra machining is needed.
- There is no need to immerse the preforms in a flammable liquid and the reactor can be located in a normal industrial setting, without the need for an explosion-proof room.

Disadvantage of recent inductively-heated thermal-gradient isobaric CVI is:

- Preforms having significantly different shapes or lateral (not thickness) dimensions may require different coil configurations.

3.3 Liquid-immersion thermal-gradient atmospheric pressure isobaric CVI

A method for rapid densification of a single porous carbon preform per run was described (Houdayer *et al*., 1981, 1984), in which the preform was placed around a cylindrical,

electrically conducting graphite susceptor, this assembly was immersed in a liquid precursor, preferably cyclohexane, C_6H_{12} (boiling temperature = 80 °C), and the reactor was heated by electromagnetic induction via a coil connected to a high frequency generator, to a temperature in the range 1,000–1,300 °C, sufficient to cause the liquid to vaporize and deposit carbon inside the pores of the preform; see Fig. 6.16. The reactor vessel is assumed to have been electrically insulating (i.e. made of glass, quartz, etc.), since the induction coil was located outside the reactor. The pressure in the reactor was essentially atmospheric. A similar approach had been previously described (Nieberlein, 1968, 1971) for the rapid deposition of SiC coatings on resistively heated, refractory metal filaments.

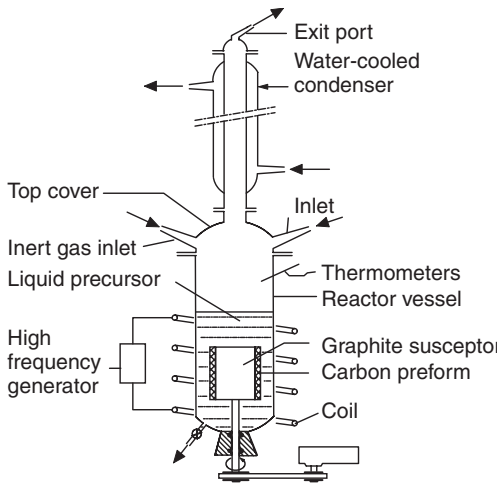

Figure 6.16 Liquid-immersion thermal-gradient inductively-heated chemical vapor infiltration reactor (Houdayer *et al*., 1984).

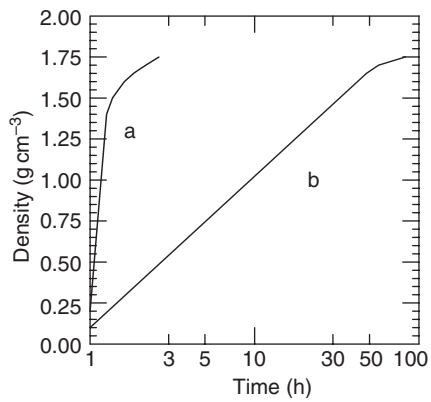

Figure 6.17 Density versus time for (a) a carbon fabric densified by liquid immersion thermal-gradient inductively-heated chemical vapor infiltration and (b) a carbon felt densified by isothermal isobaric chemical vapor infiltration, both preforms having an initial density of 0.1 g cm^{-3} (Houdayer *et al*., 1984).

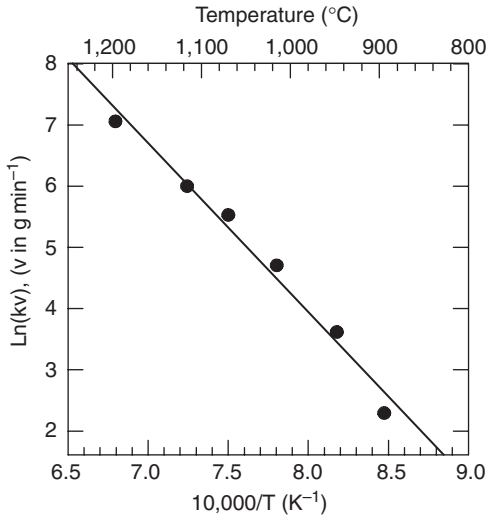

Figure 6.18 Relative rate of mass gain of C–C composite sample versus temperature in liquid-immersion inductively-heated thermal-gradient chemical vapor infiltration reactor (Narcy *et al*., 1995a; reproduced with permission of the American Ceramic Society).

Using this method, a densification time of ≈3 h was needed to reach 1.75 g cm^{-3} from an initial density of 0.1 g cm^{-3}, compared to 80 h in isothermal CVI; see Fig. 6.17. Shape, dimensional, or physical data for the densified preform or the reactor components were not provided. The electrical continuity of the preform, which has important significance regarding its coupling to the electromagnetic field, was not specified. It appears that the electromagnetic field coupled to and heated the central graphite mandrel but it is not obvious that the porous preform also coupled to the field. Preforms densified using this liquid C_6H_{12} immersion method were stated to exhibit no surface pore plugging and to have a texture and physical characteristics identical to those obtained according to the prior art; the stated application of the carbon parts was as friction materials in disk brake pads. It was stated that since carbon was first deposited in contact with the susceptor, a densification gradient was obtained from the interior to the exterior of the porous preform.

Physical properties of 2.2 cm o.d. × 1.6 cm i.d. (wall thickness 0.3 cm) × 6.5 cm long C–C composites, made from RVC 2000 carbon felt, and densified (one per infiltration run) by this method at 900–1,200 °C were recently published (Narcy *et al*., 1995a, b). The initial density was ≈ 0.1 g cm^{-3} and the final fiber fraction was <6%; these fibers were not graphitizable. The increase in mass was linear with time at each temperature. The thermal kinetics (Fig. 6.18) yielded an apparent activation energy of 2.3 eV/molecule. Final densities of 1.4–1.8 g cm^{-3}, depending on the preform used, were reached in a few hours. The deposited carbon was rough-laminar as determined by polarized-light optical microscopy and the structure was reported to be homogeneous. The matrix deposited at the lowest temperature, 930 °C, was more likely to produce a "graphite-like structure" after annealing at 2,450 °C, based on the crystallite sizes determined from X-ray diffraction.

The above immersion principle was recently used (Carroll *et al*., 1995; Thurston *et al*., 1995; Scaringella *et al*., 1996) for densification of C–C, SiC–SiC, and SiC–Si_3N_4 composites. Examples given of precursors for C infiltration were cyclohexane, n-hexane, benzene,

cyclopentane, cyclohexene, 1-hexene, gasoline, methyl cyclohexane, and toluene. Here the water-cooled copper coil was located inside the reaction chamber, which was fabricated from a non-magnetic material (e.g. quartz, glass, stainless steel, ceramic). Continuous replacement, filtering (using ceramic or charcoal filter) and cooling of the liquid precursor during densification was described. An annular 4.0 cm o.d. × 3.8 cm i.d. (wall thickness 0.1 cm) × 15.2 cm high carbon preform with an initial bulk density of 1.3 g cm^{-3} was placed around a central graphite susceptor core and densified in cyclohexane liquid. The preform was made of a plurality of overlapping sheets of conventional carbon/phenolic material in a format called involute wrap and was carbonized by heating in excess of 650 °C. The power supply was run at 30 kW and 160 kHz and preform temperatures between 900 and 1,500 °C were achieved. After 4 h, the bulk density was 1.83 g cm^{-3} (mercury porosimetry gave 2.01 g cm^{-3}); the porosity was 6.2%. From these data, a bulk mass pick-up rate of 2.5 g h^{-1} is calculated. The tube had a compressive strength of 179 MPa (26.3 ksi) and a modulus of 300 GPa (44.1 Msi). An alternate means of heating a bar-shaped preform was described, using direct-contact, d.c. or a.c. Joule heating, with the bar clamped between two copper electrodes and the whole assembly immersed in the liquid precursor. Such resistive heating results in a very different spatial power density profile compared to inductive heating (Brown *et al*., 1948; Jackson, 1962). All descriptions referred to infiltration of only one preform at a time; the precursor conversion efficiency was not provided.

A 33 cm o.d. (by ≈ 18 cm i.d. by ≈ 1.5 cm thickness, both estimated from the published photograph) C–C aircraft brake disk pad was stated to have been densified in a single 8 h cycle to a "uniform" density of 1.85 g cm^{-3} (Textron, 1994). The initial density of the disk was not provided. The refurbishment by means of densification of worn C–C rotor brake pads from F-16 military aircraft was described (Scaringella *et al*., 1996). Each rotor was a 30.5 cm diameter annular disk which was ground to half its original thickness (value not provided). Each such disk was densified by being heated between two pancake-shaped induction coils while both disk and coils were immersed in liquid C_6H_{12} (one disk per run). Heating the worn disk to an internal temperature of 950–1,100 °C for 2.0–3.5 h was generally observed to be sufficient to refurbish it to a density at least equal to that of an original equipment. The surface temperature of the disk was estimated to be approximately 800–1,100 °C during the densification runs. Total process run times were 48 h or less. Initial and final densities were not provided, but a deposited carbon matrix density of at least 1.85 g cm^{-3} was claimed. Friction coefficients, wear rates and carbon microstructures ("preferably substantially non-isotropic") at least equivalent to those in unused or conventionally refurbished brake pads were obtained. The friction and wear data were acquired using subscale (3.2 cm o.d. × 2.2 cm i.d.) test specimens. A post-densification, 2 h annealing in flowing Ar at 2,100 °C reduced the wear rate without changing the average friction coefficient.

The thermal conditions determining the preform temperature distribution in this type of liquid-immersion reactor are quite different compared to those in a flowing vapor, inductively-heated, thermal-gradient CVI reactor described in Section 2.3.2. In the liquid immersion reactor, significant convection currents exist in the boiling liquid, which cool the exterior of the preform, and significant additional cooling of the heated preform takes place during liquid immersion through the boiling of the liquid (Thurston, 1995). Axial non-uniformities in the heat transfer out of the preform may occur due to variations in the velocity and amount of vapor generated from the liquid along the length of the preform.

Advantages of liquid-immersion thermal-gradient atmospheric-pressure CVI include:

- Infiltration time of single preform is short.
- Single-cycle densification.

Disadvantages of liquid-immersion thermal-gradient atmospheric-pressure CVI include:

- Scale up to simultaneous infiltrations of multiple preforms may be challenging, due, e.g. to the "vapor lock" effect (Thurston *et al*., 1995; Scaringella *et al*., 1996). If the preforms are too close to one another, or if the walls of the reaction vessel are too close to a preform, vapor may build up, thereby displacing the liquid, greatly reducing convective heat extraction from the preform and creating a thermal hot spot and non-uniform densification.
- The precursor pressure is 1 atm or above and practically fixed, resulting in a very low gas-phase diffusivity and potentially degraded density profiles (Kotlensky, 1973; Naslain *et al*., 1989; Pierson, 1992). Atmospheric pressure CVI can additionally result in significant formation of soot and other undesirable by-products.
- Complete immersion of the preform in liquid precursor(s) is required, raising safety concerns associated with handling large amounts of flammable and/or toxic liquids which are boiling in extremely close proximity to parts maintained at 900–1,500 °C.
- Preforms having significantly different shapes and lateral dimensions may require different coil configurations.
- The preform needs to be preferably placed in a support fixture (Thurston *et al*., 1995; Scaringella *et al*., 1996), in order to firmly hold the preform within the boiling liquid with respect to the reactor and coil.

In the next section, we describe CVI using a combination of forced-flow and thermal gradient.

3.4 Forced-flow thermal-gradient atmospheric-pressure CVI

In forced-flow thermal-gradient CVI (Kotlensky, 1973; Lackey and Caputo, 1986), there is a pressure gradient impressed across one of the dimensions (usually the thickness) of the porous preform and an inverse temperature gradient across the same dimension. The temperature is coldest at the surface exposed to the high pressure (about 1–2 atm = 100–200 kPa) of the precursor and hottest at the opposing surface. The preform is heated by thermal radiation. All the precursor vapor is made to flow through the preform and the process is finished when the pressure gradient across the preform becomes too large, 0.7–1.4 atm = 70–140 kPa (Besmann *et al*., 1991), due to the closure of the flow passages through the pores. In a study of forced-flow, thermal-gradient CVI from the 1960s (Kotlensky, 1973), 0.64 cm thick, layered carbon preforms were densified for 6 h at 1,700 °C in CH_4. The densities of these preforms increased from 0.075 g cm^{-3} (felt) or from 0.5 g cm^{-3} (fabric) to 1 g cm^{-3}. In a later patent, the deposition of matrix material was stated to occur progressively from the hot surface towards the cold surface (Lackey and Caputo, 1986). This process is best suited for densification of relatively thin-walled tubes and disk-shaped preforms (one preform per run). The specially designed apparatus required is relatively complex and high-temperature fixturing and gasketing are needed. This process has been applied to the densification of SiC–SiC composites (Lackey and Caputo, 1986), including, e.g. 3.7 cm o.d. × 2.5 cm i.d. × 20 cm long SiC-Nicalon-fiber tube preforms (Stinton *et al*., 1995) and 23 cm o.d. × 0.3–1.3 cm thick T-300 carbon, SiC–Nicalon, and Nextel 480 mullite fibrous disk preforms (one preform per run) infiltrated with SiC or Si_3N_4 (Gulden *et al*., 1990).

This process was applied to the densification of 4.76 cm diameter × 0.8–1.0 cm thick carbon preforms (one preform per run), fabricated by stacking 40 layers of plain-woven T-300 carbon fiber cloth (fiber diameter 7 μm, fiber density 1.77 g cm^{-3}, 3,000 fibers/bundle) in 0°–30°–60°–90° orientation inside a perforated graphite holder (Lackey *et al*., 1995; Vaidyaraman *et al*., 1995a,b). The lay-up was compressed in a graphite punch at ≈ 900 N (91 kgf); fiber content was 46–60%vol. Preform temperature and thermal gradient could be varied by altering the height of the preform holder or the preform thickness. CH_4, C_3H_8 (propane), or C_3H_6 (propylene) diluted in H_2 were used as precursors; Ar was made to flow in the region outside the reaction chamber to protect the furnace heating elements. All infiltration runs were carried out at atmospheric pressure and terminated once the back pressure, p_b, reached 172 kPa (≈ 1.7 atm). The bottom temperature of the disk, T_{bot}, was measured with a type K thermocouple, while the initial value of the top temperature, T_{top}, was obtained from a calibration chart relating the latter to furnace power. The rate of weight gain was much higher using C_3H_6 or C_3H_8, compared to CH_4, even though CH_4 runs were carried out at higher temperatures. This was explained by the higher stability of radicals produced in methane pyrolysis. Comparing two CVI runs with (a) 50 sccm CH_4 and 50 sccm H_2, T_{top} = 1,320 °C, T_{bot} = 1,050 °C and (b) 100 sccm C_3H_6 and 100 sccm H_2, T_{top} = 1,200 °C, T_{bot} = 850 °C, the rates of weight gain, infiltration times, final densities and precursor efficiencies were (a) 0.25 g h^{-1}, 38.5 h, 1.51 g cm^{-3}, 15.4% and (b) 1.1 g h^{-1}, 8 h, 1.69 g cm^{-3}, 11.4%. The rate of weight gain increased with precursor concentration. The carbon coating thickness in micropores (around the fibers within each bundle) and macropores (between bundles and between cloth layers) was measured by means of scanning electron microscopy (SEM); see Fig. 6.19. A SiC marker was introduced (e.g. at 2, 4, 6, and 8 h) by CVI during short interruptions in the flow of C_3H_6, allowing later visualization in the SEM. The micropore coating thickness did not depend on distance from the bottom (cooler) face of the preform, although the scatter was ±30% (Fig. 6.19). The macropore coating thickness, on the other hand, was lowest at the cooler face and increased by 200% with distance towards the hotter face. No SiC was seen inside the fiber bundles, signifying that intra-bundle infiltration

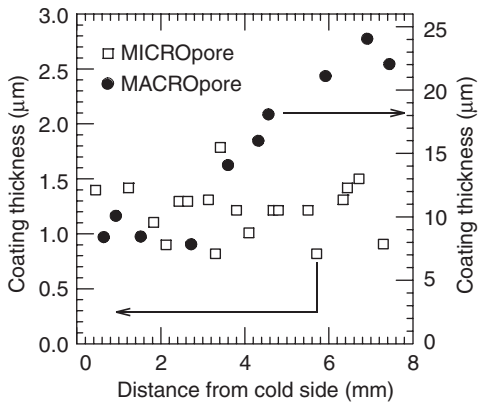

Figure 6.19 Axial variation of carbon coating thickness in micro-(□) and macro-(●) pores in 4.76 cm diameter × 1.0 cm thick C–C disk preform densified by forced-flow radiantly-heated thermal-gradient CVI (Vaidyaraman *et al*., 1995a; reproduced with kind permission from the Materials Research Society). T_{top} = 1,200 °C, T_{bot} = 850 °C (at start of run); H_2/C_3H_6 = 1.

was completed in less than 2 h and the passages within the bundles were blocked early. The highest deposition rate in the macropores, obtained in the runs with 50% C_3H_6 and 50% C_3H_8, was stated to be similar to that obtained for forced-flow thermal-gradient CVI of SiC–SiC composites and more than an order of magnitude larger than the deposition rate of 0.1–0.25 $\mu m\,h^{-1}$ for isothermal CVI of C or SiC. The large variation in deposition rate for a given processing condition was attributed to variations in fiber spacing and uneven distribution of macropores, apparently as a result of nonuniform pressure during preform compaction. The precursor conversion efficiencies were 5–24% for C_3H_6, 3–14% for C_3H_8, and 10–15% for CH_4, much higher than the typical 0.8–1.5% reported for isothermal isobaric CVI. Stopping C_3H_6/H_2 runs when $p_b = 142$ kPa (1.41 atm), the shortest densification times for a 0.75 cm thick composite were 2.75 and 3.50 h, resulting in final bulk densities of 1.64 and 1.70 $g\,cm^{-3}$, total porosities of 9.8% and 7.2% and precursor efficiencies of 18.2% and 24.4%, respectively (Vaidyaraman *et al*., 1996a,b). Using C_3H_8/H_2 and stopping the runs when $p_b = 136$ kPa (1.34 atm), the corresponding values were 7 h, 1.68 $g\,cm^{-3}$, 8.3%, and 9.0%. In the 2.75 h run, T_{bot} first increased rapidly from 820 to 950 °C within 0.5 h (attributed to reduced thermal conductivity of the gas mixture as C_3H_6 was added to H_2), stayed at 950 °C to 1.5 h, then decreased to ≈ 870 °C and increased again to 940 °C. The infiltration time decreased with increasing T_{bot} and with higher precursor concentration, and in the case of C_3H_6/H_2 runs, also with increasing total flow rate. The effect of flow rate was interpreted to indicate a CVD regime intermediate between surface reaction and gas-phase diffusion control. Density measurements of slices at different locations within the composites indicated generally lower densities at the cooler side, the effect being more pronounced (≈ 10%) for C_3H_6/H_2 runs. The measured exponential – up to 800% – increase in carbon coating thickness in macropores with distance from the cooler side of the composite was not reflected in a correspondingly large density variation (only 8–24% measured) because the majority of initial porosity was in micropores within the bundles. It was stated that p_b was a reliable indicator of the final bulk density since, for one set of experiments, these densities, in the range 1.58–1.71 $g\,cm^{-3}$, were fairly independent of the temperatures, pressures, and flow rates. However, premature crusting of the cooler preform side seen in one run, resulted in high p_b as well, even though the top 60% of the preform was not densified. SEM showed a two-layer structure of the CVD carbon matrix in some composites, but no information on whether the deposited carbon was isotropic or laminar was provided.

Advantages of forced-flow radiantly-heated thermal-gradient atmospheric-pressure CVI include:

- short densification time;
- one step densification – no intermediate grinding (Matlin *et al*., 1995);
- high precursor conversion efficiency, 3–24% for C.

Disadvantages of forced-flow radiantly-heated thermal-gradient atmospheric-pressure CVI include:

- unsuitable for complex-shaped performs;
- one preform per CVI run – scale up to multiple parts considered challenging;
- spatial density gradients may exist within the perform;
- temperature within preform varies in a complex way during densification, depending on preform architecture (Vaidyaraman, 1996a);
- requires final machining, due to deformation of the preform in the exhaust areas and to the preform becoming attached to the graphite fixturing (Matlin *et al*., 1995);
- very complex apparatus;

- requires expensive graphite fixturing; new fixturing must be made for preforms of different dimensions.

4 Summary

The CVI methods described in this review are grouped together with respective advantages and disadvantages in Table 6.1. Certain criteria for capability were chosen, for instance the published ability to densify more than one preform per run and the ability to densify relatively thick (>2.5 cm thick) preforms. Additional published CVI densification approaches, not covered here due to space limitations, were described recently (Golecki, 1997). Since different methods are at different stages of technological development, this information should be viewed as a snapshot, based on the demonstrated concepts in the literature cited herein. Certain methods may be more suitable than others for particular applications, materials (fibers and/or matrix), article shape, dimensional tolerances, intended use environment, production volume, and cost. The fields of C–C composite materials and densification of such composites continue to provide exciting and active opportunities for research and development, driven by the superior physical properties of C–Cs.

Disclaimer

To the best knowledge of the publisher, the author and the author's institution, the information contained in this chapter, which is based on published papers and patents, is accurate; however, the publisher, the author, and the author's institution assume no responsibility nor liability for errors or any consequences arising from the use of the information contained herein. Final determination of the suitability of any datum, information, idea, procedure, method, process, equipment, or product for use contemplated by any user, and the manner of that use, is the sole responsibility of the user. Materials and processes described herein could be potentially hazardous and due caution should always be exercised in the handling of materials and equipment. Expert advice should be obtained at all times when implementation is being considered. Mention of manufacturers' trademarks or trade names does not constitute endorsement by the author, the author's institution or the publisher.

Acknowledgment

Financial support by Honeywell International Inc. (formerly AlliedSignal, Inc.) of the work performed there is acknowledged.

References

Besmann, T. M., Sheldon, B. W., Lowden, R. A., and Stinton, D. P. (1991) "Vapor-phase fabrication and properties of continuous-filament ceramic composites," *Science*, **253**, 1104–1109.

Brown, G. H., Hoyler, C. N., and Bierwirth, R. A. (1948) *Theory and Application of Radio-Frequency Heating*, Van Nostrand, NY.

Buckley, J. D. and Edie, D. D. (eds) (1993) *Carbon–Carbon Materials and Composites*, Noyes Publications, Park Ridge, NJ.

Carroll, T. J., Connors, D. F., Jr., Suplinskas, R. J., and Thurston, G. S. (1995) "Method for densifying porous billets," US Patent No. 5,397,595.

Duan, Z. and Don, J. (1995) "CVI densification of Carbon–Carbon composites," *Proc. 22nd Biennial Conf. on Carbon*, American Carbon Society, San Diego, CA, July 1995, 80–81.

Golecki, I., Morris, R. C., and Narasimhan, D. (1994) "Method of rapidly densifying a porous structure," US Patent No. 5,348,774.

Golecki, I., Morris, R. C., Narasimhan, D., and Clements, N. (1995a) "Rapid densification of porous carbon–carbon composites by thermal-gradient chemical vapor infiltration," *Appl. Phys. Lett.*, **66**, 2334–2336.

Golecki, I., Morris, R. C., Narasimhan, D., and Clements, N. (1995b) "Rapid densification of Carbon–Carbon by thermal gradient chemical vapor infiltration," *Cer. Eng. & Sci. Proc.*, **16**, No. 4, 315–322.
Golecki, I., Morris, R. C., Narasimhan, D., and Clements, N. (1996) "Carbon–Carbon composites inductively heated and rapidly densified by thermal gradient chemical vapor infiltration: density distributions and densification mechanism," *Ceramic Transactions*, **79**, 135–142.
Golecki, I. (1997) "Rapid vapor-phase densification of refractory composites," invited review paper, *Materials Science and Engineering: Reports*, **R20**, No. 2, 37–124.
Golecki, I. and Narasimhan, D. (1998) "Method for measuring the deposition, densification or etching rate of an electrically conductive body," US Patent No. 5,747,096.
Golecki, I., Xue, L., Leung, R., Walker, T., Anderson, A. F., Dewar, D. M., Duncan, C. K., and van Horik, J. (1998) "Properties of high thermal conductivity Carbon–Carbon composites for thermal management applications," in I. Golecki, E. Kolawa, and B. Gollomp (eds), *Proc. 1998 High Temperature Electronic Materials, Devices and Sensors Conference*, San Diego, CA, February 1998, IEEE, Piscataway, NJ, 190–195.
Golecki, I., Xue, L., Dewar, D. M., Anderson, A. F., Duncan, C. K., van Horik, J., Fuentes, K., Rahman, F., and Walker, T. (2000) "Oxidation study of bare and protected Carbon–Carbon composites for accelerated lifetime testing," in S. Loud, V. Karbhari, D. O. Adams, and A. B. Strong (eds), *Proc. 45th International SAMPE Symposium and Exhibition*, Long Beach, CA, May 2000, Society for the Advancement of Material and Process Engineering, 671–682.
Golecki, I. and Narasimhan, D. (2001) "Novel real-time method for measuring the densification rate of Carbon–Carbon fiber-matrix composites and other articles," invited paper, in M. Singh and T. Jessen (eds), *Ceramic Engineering & Science Proc*. **22**, 3, 103–114.
Grove, A. S. (1967) *Physics and Technology of Semiconductor Devices*, John Wiley, New York, ch. 1.
Gulden, T. D., Kaae, J. L., Norton, K. P., and Thompson, L. D. (1990) "Forced-flow thermal-gradient chemical vapor infiltration (CVI) of ceramic matrix composites," *Electrochem. Soc. Proc.*, **90–12**, 546–552.
Hitchman, M. L. and Jensen, K. F. (eds) (1993) *Chemical Vapor Deposition – Principles and Applications*, Academic Press, London.
Houdayer, M., Spitz, J., and Tran-Van, D. (1981) "Increasing the density of a porous structure," French Patent No. 81 22163–26/11/81.
Houdayer, M., Spitz, J., and Tran-Van, D. (1984) "Process for the densification of a porous structure," US Patent No. 4,472,454.
Hüttinger, K. J. (2003) "Fundamentals of chemical vapor deposition in hot wall reactors," ch. 4, in P. Delhaès (ed), *World of Carbon*, Vol. 3, *Fibers and Composites*, Taylor and Francis, London.
Jackson, J. D. (1962) *Classical Electrodynamics*, John Wiley and Sons, Inc., New York.
Kotlensky, W. V. (1971) "A review of CVD carbon infiltration of porous substrates," *Proc. 16th National Symposium of the Society of Aerospace, Materials & Process Engineers (SAMPE)*, Anaheim, CA, April 1971, 257–265.14.
Kotlensky, W. V. (1973) "Deposition of pyrolytic carbon in porous solids" in P. L. Walker, Jr. and P. A. Thrower (eds), *Chemistry and Physics of Carbon*, Marcel Dekker Inc., New York, **9**, 173–262.
Lackey, W. J. (1989) "Review, status, and future of the chemical vapor infiltration process for fabrication of fiber-reinforced ceramic composites," *Ceram. Eng. Sci. Proc.*, **10**, No. 7–8, 577–584.
Lackey, W. J. and Caputo, A. J. (1986) "Process for the preparation of fiber-reinforced ceramic composites by chemical vapor deposition," US Patent No. 4,580,524.
Lackey, W. J., Vaidyaraman, S., Freeman, G. B., Agrawal P. K., and Langman, M. D. (1995) "Rapid fabrication of carbon–carbon composites," *Ceram. Eng. Sci. Proc.*, **16**, No. 4, 299–306.
Lieberman, M. L. and Noles, G. T. (1973) "Gas analysis during the chemical vapor deposition of carbon," *Proc. 4th International Conference on Chemical Vapor Deposition*, Electrochemical Society, Boston, MA, Oct. 1973, 19–29.
Lieberman, M. L., Curlee, R. M., Braaten F. H., and Noles, G. T. (1975) "CVD/PAN felt carbon/carbon composites," *J. Composite Materials*, **9**, 337–346.
Loll, P., Delhaès, P., Pacault, A., and Pierre, A. (1977) "Diagramme d'existence et propriétés de composites carbone-carbone," *Carbon*, **15**, 383–390.

Lovell, D. R. (ed.) (1995) *Carbon and High Performance Fibres Directory and Databook*, 6th edn., Chapman & Hall, London.
Marinkovic, S. and Dimitrijevic, S. (1987) "Process of infiltration of porous carbon bodies by CVD carbon and properties of resulting composites," *Journal de Chimie Physique*, **84**, 1421–1430.
Matlin, W. M., Stinton, D. P., Besmann, T. M., and Liaw, P. K. (1995) "Optimization of bundle infiltration in the forced chemical vapor infiltration (FCVI) process," *Mat. Res. Soc. Symp. Proc.*, **365**, 309–315.
Narcy, B., Guillet, F., Ravel, F., and David, P. (1995a) "Characterization of carbon–carbon composites elaborated by a rapid densification process," *Ceramic Transactions*, **58**, 237–242.
Narcy, B., David, P., and Ravel, F. (1995b) "Elaboration of C/C and C/BN composites by a rapid densification process," *Silicates Industriels*, **7–8**, 199–202.
Naslain, R., Langlais, F., and Fédou, R. (1989) "The CVI-processing of ceramic matrix composites," *J. de Physique*, **50**, *Colloque C5, Suppl. to No. 5*, 191–207.
Nieberlein, V. A. (1968) "Deposition of silicon carbide from liquid compounds," *SAMPE Journal*, **4**, No. 6, 72–74.
Nieberlein, V. A. (1971) "Method for depositing carbide compound," US Patent No. 3,554,782.
Pierson, H. O. (1992) *Handbook of Chemical Vapor Deposition (CVD)*, Noyes Publications, Park Ridge, NJ.
Pierson, H. O. and Lieberman, M. L. (1975) "The chemical vapor deposition of carbon on carbon fibers," *Carbon*, **13**, 159–166.
Savage, G. (1993) *Carbon–Carbon Composites*, Chapman & Hall, Cambridge, UK.
Scaringella, D. T., Connors, D. E., Jr. and Thurston, G. S. (1996) "Method for densifying and refurbishing brakes," US Patent No. 5,547,717.
Sheehan, J., Buesking, K. W., and Sullivan, B. J. (1994) "Carbon–carbon composites," *Ann. Rev. Matls. Sci.*, **24**, 19–44.
Stinton, D. P., Besmann, T. M., Matlin, W. M., Starr, T. L., and Curtain, W. A. (1995) "Forced chemical vapor infiltration of tubular geometries: modeling, design and scale-up," *Mat. Res. Soc. Symp. Proc.*, **365**, 317–324.
Stoller, H. M. and Frye, E. R. (1972) "Processing of Carbon–Carbon composites – an overview," *SAMPE Quarterly*, **3**, No. 3, 10–22.
Stoller, H. M., Butler, B. L., Theis, J. D., and Lieberman, M. L. (1974) "Carbon fiber reinforced-carbon matrix composites," in J. Weeton and E. Scala (eds), *Composites: State of the Art*, Met. Soc. of AIME, *Proc. 1971 Fall Meeting of the Metallurgical Society of AIME*, Detroit, MI, 69–136.
Tesner, P. A. (1984) "Kinetics of pyrolytic carbon formation," ch. 2 in P. A. Thrower (ed.), *Chemistry and Physics of Carbon*, Marcel Dekker, Inc., New York, **19**, 65–161.
Textron Specialty Materials (1994) "Brake disc technology," news release, *Aerospace Products*, Fall 1994, 10.
Thiele, E. W. (1939) "Relation between catalytic activity and size of particle," *Industrial and Engineering Chemistry*, **31**, 916–921.
Thomas, C. R. (ed.) (1993) *Essentials of Carbon–Carbon Composites*, Royal Society of Chemistry, Cambridge, UK.
Thurston, G. S., Suplinskas, R. J., Carroll, T. J., Connors, D. F., Jr., Scaringella, D. T., and Krutenat, R. C. (1995) "Apparatus for densification of porous billets," US Patent No. 5,389,152.
Vaidyaraman, S., Lackey, W. J., Agrawal, P. K., Freeman, G. B., and Langman, M. D. (1995a) "Rapid processing of Carbon–Carbon composites by forced flow-thermal gradient chemical vapor infiltration (CVI)," *Mat. Res. Soc. Symp. Proc.*, **365**, 325–330.
Vaidyaraman, S., Lackey, W. J., Freeman, G. B., Agrawal, P. K., and Langman, M. D. (1995b) "Fabrication of Carbon–Carbon composites by forced flow-thermal gradient chemical vapor infiltration," *J. Mater. Res.* **10**, 1469–1477.
Vaidyaraman, S., Lackey, W. J., Agrawal, P. K., and Miller, M. A. (1996a) "Carbon/carbon processing by forced flow-thermal gradient chemical vapor infiltration using propylene," *Carbon*, **34**, 347–362.
Vaidyaraman, S., Lackey, W. J., and Agrawal, P. K. (1996b) "Carbon/carbon processing by forced flow-thermal gradient chemical vapor infiltration (FCVI) using propane," *Carbon*, **34**, 609–617.